

Microstructural Effects Governing the Fracture Behavior of Al-Li-Cu-Mg Alloy 8090

T. S. SRIVATSAN*, T. A. PLACE** and
T. S. SUDARSHAN***

*Dept. of Mechanical Engineering, The University of Akron, Akron,
Ohio 44325, USA

**Dept. of Mechanical Engineering, University of Idaho, Moscow,
Idaho 83843, USSR

***Materials Modification Inc., Falls Church, Virginia 22044, USA

ABSTRACT

The effect of microstructure on the fracture behavior of high strength, low-density Al-Li-Cu-Mg alloy 8090 was investigated. A change in fracture mode was observed with reference to direction of testing. Such results are interpreted in terms of the grain structure of the material and the nature, distribution and morphology of the second-phase particles. The overall fracture process is discussed in terms of several competing mechanistic effects involving matrix microstructural features, deformation characteristics of the matrix resulting in large stress concentrations at the grain boundary, presence of large grain boundary particles and microstructural damage. The role of stress on particle fracture and the contribution from matrix deformation characteristics are highlighted.

INTRODUCTION

One of the techniques that can significantly improve both aircraft performance and efficiency is through the reduction of structural weight. This can be accomplished through reductions in density or improvements in strength, stiffness of skin material, durability and damage tolerance (Sawtell *et al.*, 1984). The renewed interest in low density lithium-containing aluminum alloys as attractive alternatives to existing high strength precipitation hardenable aluminum alloys for stiffness-critical airframe structures stems from weight savings and combinations of high strength, increased stiffness and improved thermal stability. Several recent studies (Starke, Jr. 1984, Baker *et al.*, 1986), have shown that a reduction in density and an improvement in elastic modulus which result from lithium additions to aluminum are far more effective in improving performance and fuel economy than commensurate improvements in other secondary properties.

While aluminum-lithium alloys look potentially attractive for use in aircraft structural applications, their ductility and fracture toughness compare unfavorably with the conventional aluminum alloys at equivalent strength levels. This problem arises on account of their susceptibility to grain boundary fracture. This fracture process is generally dictated by several synergistic and mutually competitive mechanisms involving: (a) the presence of a high density of coarse grain boundary precipitates, often a more stable phase than the matrix strengthening phase (Vasudevan *et al.*, 1986), (b) presence of coarse constituents from ingot casting

(Vasudevan et al., 1984), (c) segregation of tramp elements such as sodium, potassium and sulphur to the grain boundaries (Vasudevan et al., 1985), (d) strain localization in coarse slip bands due to heterogeneity of slip (Unwin & Smith, 1969) and (e) the exacerbating effect of precipitate-free zones which aids in enhancing the stress concentration at grain boundaries and grain boundary triple junctions (Lin et al., 1982). The localization of strain results in the build-up of high stresses at the grain boundaries and grain boundary triple junctions. The high stress concentration at the grain boundaries promotes easy separation thus resulting in low energy intergranular fracture.

Strain localization which results from dislocation shearing of the matrix precipitates can be minimized by: (i) overaging to produce incoherent precipitates, (ii) refining the grain structure, and (iii) alloying to improve the overall homogeneity of deformation. Overaging results in the precipitation of equilibrium phases at grain boundaries with concomitant formation of wide precipitate-free zones which are detrimental to ductility. A refinement in grain structure through reductions in grain size decreases the slip length and reduces the stress concentration at grain boundaries. Further, the small grains enhance multiple slip and assist in promoting homogeneous deformation. Since the deformation of precipitation hardenable aluminum alloys is governed by the interaction of dislocations with the strengthening precipitates, modifying the nature, size, coherency and distribution of the precipitates present through alloying is an attractive method for eliminating strain localization effects.

The object of this paper is to present the influence of intrinsic microstructural effects on the fracture behavior of a quaternary AlLi alloy in the peak-aged, maximum strength condition. High strength aluminum alloy 8090 was chosen for this study because of its similarity to the existing commercial aluminum alloys and its potential use in aerospace applications. The micromechanisms governing the fracture process are discussed in light of competing effects involving synergistic interactions among the intrinsic microstructural features, matrix deformation characteristics, brittleness of grain boundary precipitates and grain boundary failure.

MATERIALS AND METHODS

Materials

The Al-2.8 Li-1.3 Cu-0.7 Mg-0.12 Zr alloy 8090 investigated in this study was provided by the U.S. Navy, Naval Surface Weapons Center. The alloy was in the form of an extruded plate of cross-section 100 mm x 25 mm (4 in x 1 in) in the maximum strength, peak-aged condition. Details of the T851 processing treatment are provided elsewhere.

Experimental Methods

Metallographic samples were cut from the three orthogonal directions of the extruded plate, mounted in bakelite and wet-ground on 320, 400 and 600 grit silicon carbide (SiC) paper using water as lubricant and then mechanically polished with 1 micron and 0.05 micron alumina-based lubricant. Grain morphology was revealed using Keller's etch. Size and distribution of the soluble phases were determined using a hot (50°C) 10 percent orthophosphoric acid solution as the etchant. A hot bromine etch procedure was used to analyze the size, morphology and distribution of the insoluble and high temperature precipitating phases. The etched specimens were examined by scanning electron microscopy.

Tensile tests were performed on (ASTM Standard E-8) smooth, cylindrical specimens of 35 mm gauge length and 6.35 mm diameter. The stress axis of the cylindrical samples was parallel (longitudinal) or perpendicular (transverse) to the extrusion direction. The tests were performed on a closed-loop servohydraulic testing machine with an initial strain rate of 6×10^{-4} per second. Fracture surfaces of the deformed tensile samples were examined in a scanning electron microscope (SEM) so as to determine the predominant fracture mode and to characterize the fine scale features on the fracture surface.

RESULTS AND DISCUSSION

Grain Structure

Optical microscopy of the Al-Li-Cu-Mg Alloy plate revealed the material to be partially recrystallized with the unrecrystallized grains flattened and elongated in the longitudinal direction, as a consequence of deformation introduced during extrusion. The transverse grains appeared to have a large aspect ratio. An optical micrograph of the longitudinal section is shown in Figure 1. The grain and subgrain boundaries were decorated with a fine dispersion of second-phase particles that are: (a) the equilibrium phases [δ (AlLi), S(Al_2CuMg) and T-type ($\text{Al}_x\text{Cu}_y\text{Li}_z$)], (b) the coarse iron-rich intermetallics, and (c) the magnesium-rich insoluble phases.

At higher magnification, the insoluble and partially soluble constituent particles were observed to be stratified and distributed along the extrusion direction of the plate. At regular intervals along the longitudinal (extrusion) direction of the as-received plate, clustering of the constituent particles was observed. The distribution and morphology of larger insoluble constituent particles was revealed by bromine etching (Figure 2). The density of these particles was observed to be greater in the longitudinal direction than in the transverse direction of the extruded plate (Srivatsan, 1987).

Particles and Phases Present in the Al-Li-Cu-Mg Alloy

The elements iron (0.05 pct) and silicon (0.02) pct in the alloy are impurities. During ingot solidification and subsequent processing, these impurities precipitate as insoluble constituent phases, Al_3Fe and $\text{Al}_7\text{Cu}_2\text{Fe}$. Zirconium additions result in the formation of metastable β' (Al_3Zr) phase which are spherical in morphology and can effectively pin the grain and subgrain boundaries. The cubic Al_3Zr (β') phase also known as a dispersoid has an Ll_2 structure and nucleates heterogeneously on dislocations and grain boundaries (Rioja and Ludwiczak, 1986). The β' particles (Al_3Zr) are coherent with the aluminum matrix and aids in: (i) retarding subgrain boundary migration and coalescence, (ii) suppresses recrystallization, (iii) controls grain growth, (iv) stabilizes the subgrain structure and (v) provides additional strengthening [12]. The major strengthening precipitates in the ternary Al-Cu-Li alloys are δ' (Al_3Li), T_1 (Al_2CuLi), θ'' (Al_2Cu) and θ' (Al_2Cu) (Galbraith et al., 1986, Srivatsan et al., 1986, Crooks, 1984), where θ'' and θ' are analogous to the intermediate precipitates found in binary aluminum-copper alloys. In the peak-aged, maximum strength condition the Al-Li-Cu alloys contain precipitate free zones along the grain and subgrain boundaries (Srivatsan et al., 1986). Magnesium additions to Al-Li alloys improves the strength of the alloy by co-precipitating with δ' (Al_3Li) and/or incorporating lithium to form coherent and partially coherent ternary phases. Co-precipitation is effective because it increases the strength of the alloy and promotes homogeneous deformation. Besides, magnesium reduces the solubility of lithium in the matrix during the early stages of aging and increases the volume fraction of the coherent, ordered strengthening precipitate, δ' (Al_3Li) (Crooks and Starke, 1984). Magnesium also provides an increment of solid solution strengthening and eliminates the formation of precipitate-free zones (PFZ's) through the precipitation of S'' and S' (Al_2CuMg) phases near the grain boundaries.

Fracture Behavior:

Examination of the monotonic fracture surfaces in the scanning electron microscope is helpful in elucidating microstructural effects on the fracture properties of alloy 8090. Extensive fractography of the fracture surfaces of both the longitudinal and transverse orientations revealed: (i) transgranular shear failure, (ii) cracking along the grain boundaries or intergranular failure, (iii) intersubgranular failure along the subgrain boundaries, and (iv) void formation at the grain and subgrain boundaries.

On a macroscopic scale, tensile fracture of the peak-aged AA8090 in the longitudinal direction was predominantly shear. The fracture surface was oriented approximately 45 degrees to the major stress axis, following the plane of maximum shear stress (Figure 3a). The shear-type of fracture tends to minimize necking and thus the triaxial state of stress and hydrostatic component that occurs in a necked region (Feng *et al.*, 1984). Consequently, void nucleation at the coarse constituent and intermediate size dispersoid particles is affected.

Long secondary cracks, or ledges were observed on the fracture surfaces, separating the transgranular and intergranular regions, with the crack plane oriented parallel to the loading axis, i.e., the extrusion direction (Figure 3b). The tendency toward localized inhomogeneous planar deformation due to the interaction of mobile dislocations with the ordered coherent and partially coherent precipitate particles dispersed in the matrix of lithium-containing aluminum alloys results in strain localization. For the alloy (Al-Li-Cu-Mg) in the aging condition (peak-aged) studied, the coarse planar slip bands resulting from the interaction of dislocations with the precipitate particles impinge upon grain boundaries and causes strain concentration or localization at their point of impingement on the grain boundary. The magnitude of strain concentration in the vicinity of grain boundaries depends on the slip length. The high concentration of strain due to localized planar deformation causes a large stress build-up at the grain boundary. Stress concentration accelerates the fracture process through the initiation of microcracks at the grain boundary resulting in the formation of ledges. A schematic of the ledge type intergranular fracture is illustrated in Figure 4.

On a macroscopic scale, fracture of the transverse sample was essentially normal to the stress axis (Figure 5a). Lamellar cracks were observed separating the transgranular and intergranular regions and extending down the fracture surface parallel to the loading direction (Figure 5b). The spacing between the lamellar cracks is associated with fracture along the grain boundaries. The lateral separation of grains occurs under the action of triaxial stresses in plane strain and minimizes the constraints imposed by the neighboring grains during plastic deformation. The lateral separation results in:

- (i) macroscopic cracking along the recrystallized and unrecrystallized grain boundaries (Figure 6a), and
- (ii) microscopic cracking along the individual subgrains (Figure 7a).

The fracture path along the grain and subgrain boundaries is shown diagrammatically in Figure 6b and Figure 7b. The transgranular fracture regions were covered with a network of very fine dimples. These fine dimples are associated with the iron- and silicon-rich constituents, the zirconium dispersoids, and the equilibrium δ (AlLi) and T-type ($Al_xCu_yLi_z$) precipitates.

Participation of Particles in the Fracture Process

The intermetallics in this alloy are the iron-rich particles and the magnesium-rich insoluble phases. During plastic deformation, nucleation of cracks occurs by: (i) the

cracking of coarse constituent particles, (ii) particle-matrix interface separation, and (iii) separation at areas of poor inter-particle bonding (Van Stone *et al.*, 1985). Interfacial strength is a dominant factor in crack nucleation. There are, however, several other factors which though secondary and indirect compared to particle-matrix separation and interfacial strength, contribute to the void initiation process. These include: (a) size of the second-phase particles; (b) particle shape and volume fraction; (c) particle strength in which case void initiation occurs by particle cracking; (d) particle location and distribution (Thompson, 1987). Void initiation at the second-phase particles is also influenced by: (1) inclusion size, (2) state of stress and local strain, or both and (3) the local-deformation modes which cannot be generalized. The presence of fairly large-sized second-phase particles in AA8090 facilitates the nucleation of cracks at low stresses. Void nucleation at a second-phase particle occurs when the elastic energy in the particle exceeds the surface energy of the newly formed void (Gurland and Plateau, 1963). For the case of spherical particles, the critical stress for particle cracking is:

$$\sigma = (6\gamma E/q^2d)^{0.5} \quad (1)$$

where γ is the surface energy of the particle, q is the stress concentration factor at the particle, E is the Young's Modulus of the particle, and d is the particle diameter.

While satisfaction of Equation (1) is a necessary condition for void initiation, it must also be aided by a stress on the particle/matrix interface in excess of the interfacial strength (Argon *et al.*, 1975). When the stress at the particle/matrix interface (σ_1) reaches a critical value, void nucleation occurs by interface separation. The interface stress (σ_1) at a particle comprised of the applied stress, σ_A , and the normal stress due to blocked slip bands, (σ_p).

$$\sigma_1 = \sigma_A + \sigma_p = \sigma_A + kF(r)^{0.5} \quad (2)$$

In equation (2), σ_p is equated to the product of the constant, k , the flow stress F , and the square root of the slip-band length, r ,

Void nucleation occurs provided sufficient elastic energy is available to create new void surfaces and a critical value of σ_1 is reached. Furthermore, due to the presence of a fairly large volume fraction of second-phase particles in the alloy there exists an intrinsic particle-size effect on void nucleation. The influence of particle size is caused by the interaction of stress fields of closely spaced inclusions.

Coalescence of the microvoids is the last stage in the fracture process. During coalescence void-void interactions occur during which period void growth and strain localization effects are accelerated. In this alloy, void coalescence can result from the formation of void sheets at the small second-phase particles (at the Al_3Zr dispersoid) in conjunction with void impingement, that is, by voids growing until they touch. Since the number of microconstituents (inclusions and constituent particles) is large, some of the large voids which are created by fracture of the iron-rich intermetallic particles coalesce by impingement. The more widely separated voids coalesce by the formation of void sheets. Formation and coalescence of microvoids initiated at the coarse grain boundary precipitates results in dimple-formation type intergranular fracture (Figure 7). The transgranular fracture regions comprised of pronounced cracking along the sub-grain boundaries, parallel to the major stress axis.

The subgrains in the unrecrystallized regions have a marked influence on the fracture characteristics of AA8090 and are well developed. Due to a low degree of misorientation between neighboring subgrains, the impact of grain boundaries as barriers to dislocation motion is reduced. This tends to increase the "effective" slip length with concomitant reduction in ductility. The poor ductility of alloy 8090 in the peak-aged condition is not a consequence of planar deformation per se, but due to the presence of coarse grain boundary precipitates. Micro-dimples were observed on

the intersubgranular fracture surface (Figure 7). The dimples are the result of the presence of smaller second-phase particles, that is, the zirconium dispersoids (Al_3Zr), and the T-type ($Al_xCu_yLi_z$) precipitates. The equilibrium δ (AlLi) and Al_2MgLi phases along the grain and subgrain boundaries promote intergranular void coalescence.

Deformation and Microstructural Effects on Fracture

The presence of ordered coherent and partially coherent precipitate particles [$\delta'(Al_3Li)$, $T_1(Al_2CuLi)$, $\theta'(Al_2Cu)$ and $S'(Al_2CuMg)$] in the alloy enhances planar slip deformation within the matrix. The concentration of deformation in intense planar slip bands leads to strain localization at their point of impingement on grain boundaries. The localized planar deformation produces large stress concentrations at the grain boundary. The increased strength of the age-hardened matrix in the peak-aged condition renders nucleation of flow across the boundary difficult. This effect coupled with concentration of stress and the presence of coarse grain boundary precipitates accelerates the fracture process through enhanced microcrack formation at the grain boundaries and concomitant low ductility; as compared to conventional aluminum alloys of comparable strength. Void initiation results at the intersection of a slip band and a coarse grain boundary precipitate (Figure 8). The applied stress assists in the growth of voids. Linking of similar voids is an additional factor that promotes and/or enhances intergranular fracture.

CONCLUSIONS

While specific results and implications relevant to the micromechanisms of fracture in this quaternary alloy has been presented in the discussion, the general conclusions of this study are summarized as follows:

- (a) Fracture in the maximum strength, peak-aged condition was by low energy intergranular and intersubgranular separation for both the longitudinal and transverse orientations.
- (b) A major contribution to the intergranular failure process is the formation and linking of microvoids at the coarse grain boundary precipitate particles.
- (c) "Planar Slip" deformation leading to strain localization at grain boundaries in conjunction with grain boundary failure results in low values of ductility. The overall fracture process is governed by a complex interplay of several factors involving the matrix deformation characteristics, the presence of coarse microconstituents dispersed in the matrix and along the grain boundaries, and grain boundary failure.

Acknowledgements:

This work was supported by the U. S. Navy, Naval Surface Weapons Center under Contract No. N60921-86-M-7570. The authors thank Ms. Karen Ober and Mrs. Sandra Collins for typing the manuscript.

REFERENCES

- Aluminum-Lithium Alloys IV (1987): Proceedings of the Fourth International Conference on Aluminum-Lithium Alloys, Paris, France (in press).
- Argon, A. S., J. Im and A. Needleman (1975): Metallurgical Transactions, Vol. 6A, p. 825.
- Baker, C.P., J. Gregson, S. J. Harris, and C. J. Peel, (editors), (1986) Aluminum-Lithium Alloys III: Proceedings of the Third International Conference on Aluminum-Lithium Alloys, Institute of Metals, London, England.

Crooks, R. E. and E. A. Starke, Jr. (1984): Metallurgical Transactions, Vol. 15A, p. 1367.

Feng, W. X., F. S. Lin and E. A. Starke, Jr. (1984): Metallurgical Transactions, Vol. 15A, p. 1209.

Gurand, J. and J. Plateau (1963): Transactions of ASM, Vol. 56, p. 442.

Galbraith, J. M., M. H. Tosten and P. R. Howell (1987): Journal of Materials Science, Vol. 22, p. 27.

Lin, F. S., S. B. Chakraborty and E. A. Starke, Jr. (1982): Metallurgical Transactions, Vol. 13A, p. 401.

Rioja, R. J., E. A. Ludwiczak (1986): in Aluminum Lithium Alloys III, Proceedings of the Third International Conference on Aluminum-Lithium Alloys, C. Baker, S. J. Harris, B. Noble and C. J. Peel (editors), Institute of Metals, London.

Sawtell, R. R., P. E. Bretz, J. I. Petit and A. K. Vasudevan (1984): in Proceedings of 1984 SAW Aerospace Congress and Exposition, October, Long Beach, CA.

Srivatsan, T. S. (1987): "Microstructural Compatibility of an Al-Li-Cu-Mg Alloy Exposed to Corrosive Environments," Final Report, U.S. Navy, Naval Surface Weapons Center, Contract No. N60921-M-7570.

Srivatsan, T. S., E. J. Coyne, Jr., and E. A. Starke, Jr. (1986): Journal of Materials Science, Vol. 21, p. 1553.

Starke, Jr., E. A. and T. H. Sanders, Jr. (editors), (1984) Aluminum-Lithium Alloys II: Proceedings of the Second International Conference on Aluminum-Lithium Alloys, Monterey, AIME, Warrendale, PA.

Thompson, A. W. (1987): Metallurgical Transactions, Vol. 18A, p. 1877.

Unwin, P.N.T. and G.C. Smith (1969): J. Institute of Metals, Vol. 97, p. 299.

Van Stone, R. H., T. B. Cox, J. R. Low and J. A. Psioda (1985): International Metals Reviews, Vol. 30, No. 4, p. 157.

Vasudevan, A. K., E. A. Ludwiczak, S. F. Baumann, P. R. Howell, R. D. Doherty and M. M. Kersker (1986): Materials Science and Technology, Vol. 2, p. 1205-1209.

Vasudevan, A. K., A. C. Miller and M. M. Kersker (1984): in Aluminum-Lithium Alloys II, Proceedings of the Second International Conference on Aluminum-Lithium Alloys, T. H. Sanders, Jr., and E. A. Starke, Jr., (editors), AIME, Warrendale, PA, p. 81.

Vasudevan, A. K., E. A. Ludwiczak and S. F. Baumann (1985): Materials Science and Engineering, Vol. 72, L-25.

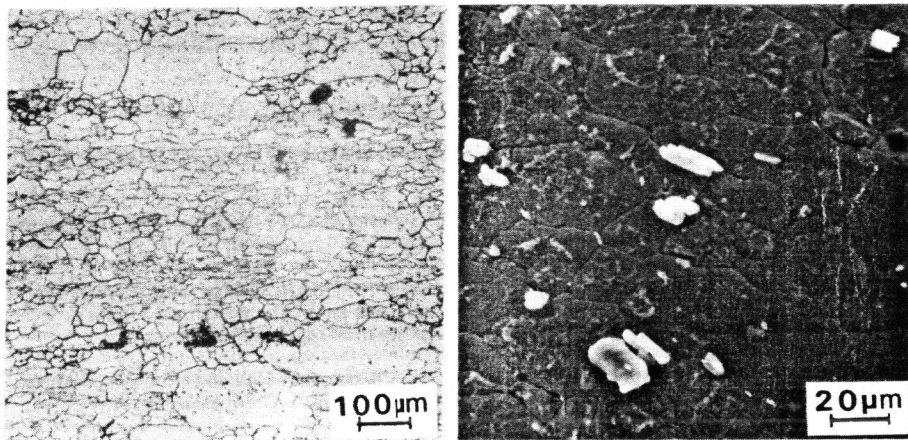


Figure 1. Optical micrograph showing grain structure along the longitudinal section of the extruded plate.

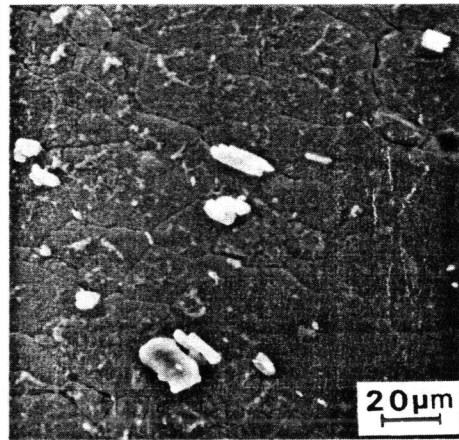


Figure 2. Scanning electron micrograph showing the morphology and distribution of the larger insoluble constituent particles on bromine-etched surface.

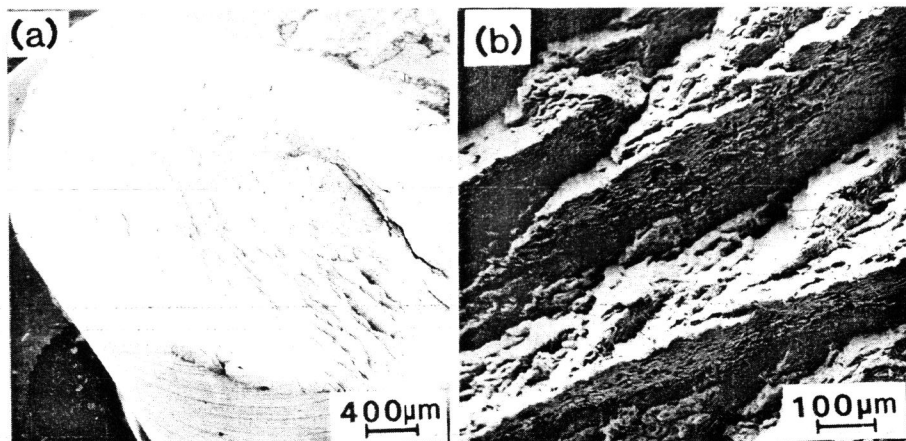


Figure 3. Scanning electron micrograph of the fracture surface of the longitudinal tensile sample showing: (a) shear-type fracture, and (b) high magnification showing large secondary cracks or ledges parallel to the extrusion direction.

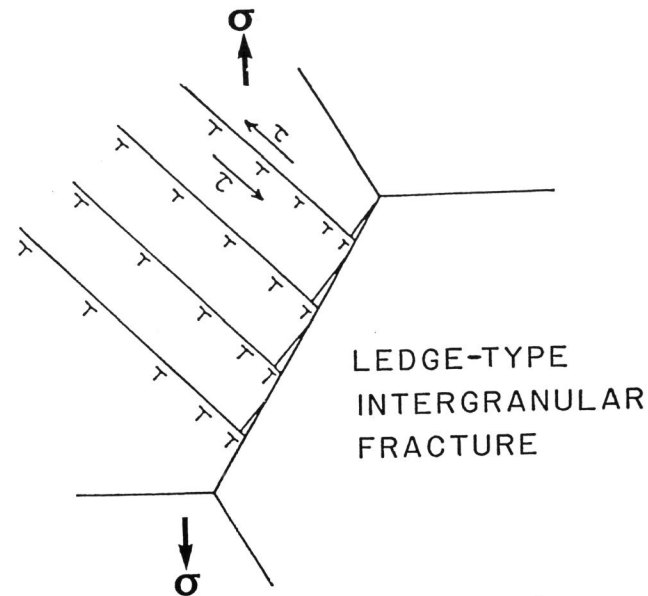


Figure 4. Schematic representation of the ledge-type intergranular fracture process.

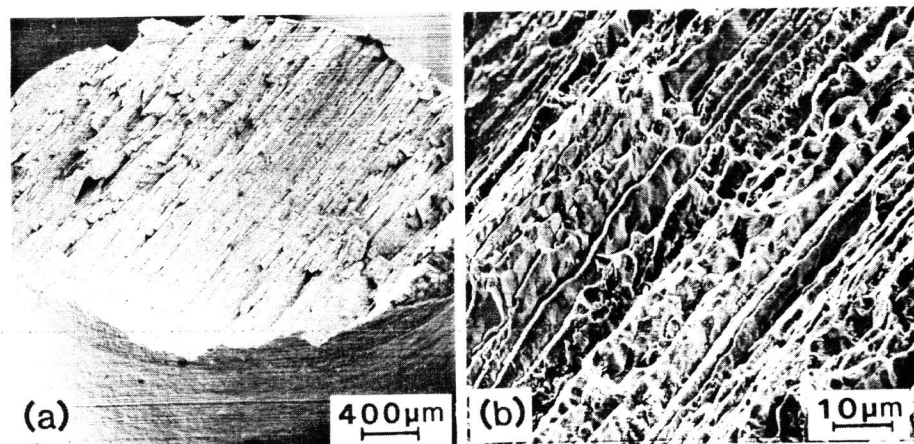


Figure 5. Scanning electron micrograph of the fracture surface of the transverse tensile sample showing: (a) fracture normal to the stress axis, and (b) lamellar cracks parallel to the major stress axis, T351 condition.

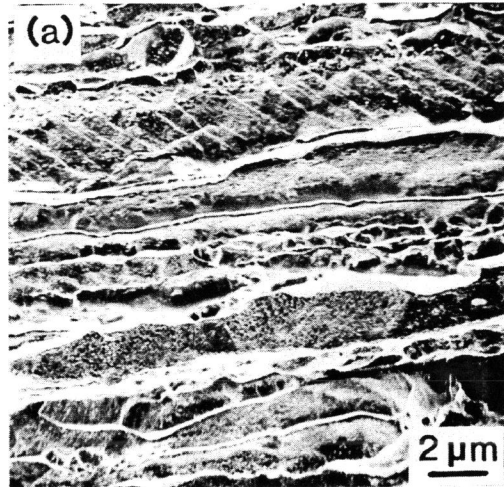


Figure 6 (a) Scanning electron micrograph of the transverse tensile sample showing intergranular cracking along the large unrecrystallized grain boundaries with fine ductile dimples on the transgranular fracture surface.

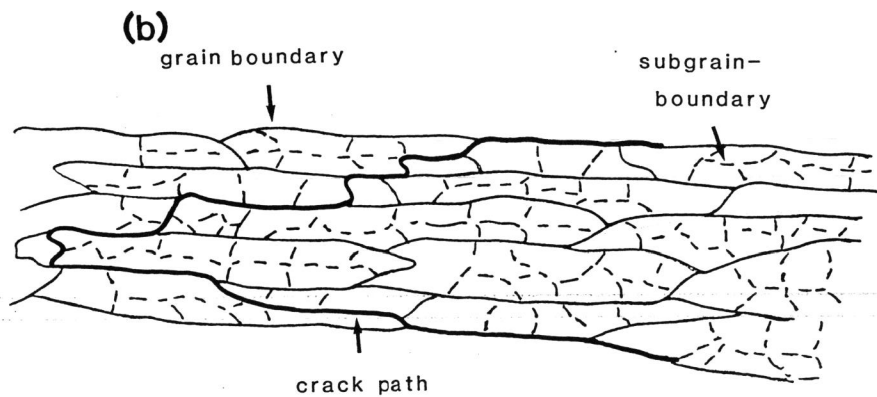


Figure 6 (b) Schematic showing failure mode along the unrecrystallized grain boundaries.

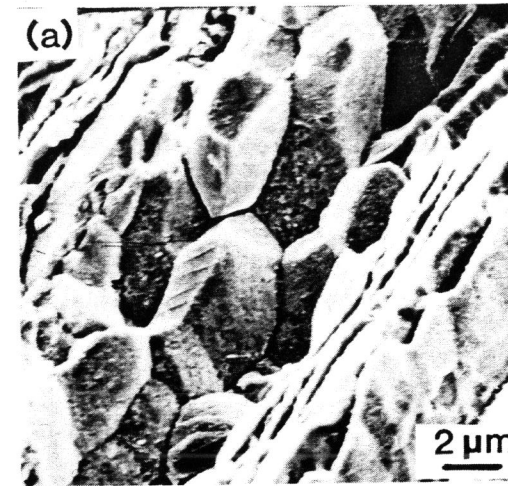


Figure 7 (a) High magnification fractograph of ridge showing intergranular cracking along the subgrain boundaries.

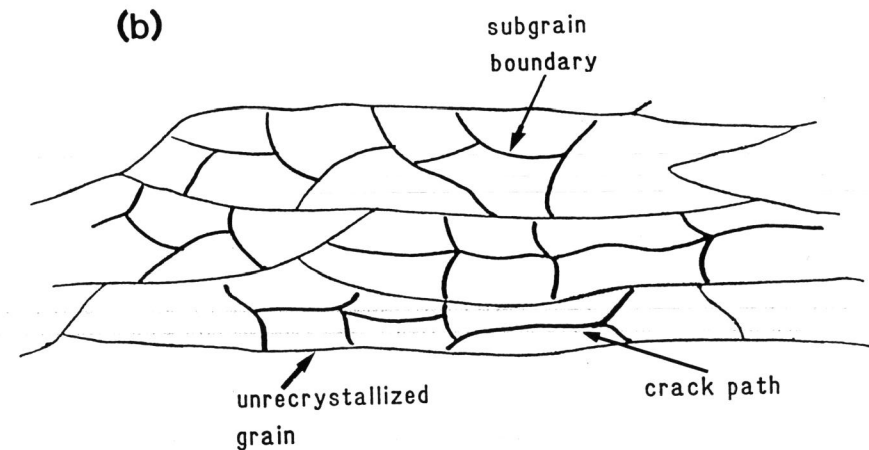


Figure 7 (b) Schematic showing intergranular cracking along the subgrains within an unrecrystallized grain.